PAPER

Calculating and assigning rovibrational energy levels of $(^{15}N_2O)_2$, $(^{15}N^{14}NO)_2$, $^{14}N_2O–^{15}N_2O$ and $^{15}N^{14}NO–^{15}N_2O$

James Brown, Xiao-Gang Wang and Tucker Carrington Jr.

In this paper we report transition frequencies and rotational constants computed for several isotopologues of the nitrous oxide dimer. A previously reported intermolecular potential, the symmetry adapted Lanczos algorithm and an uncoupled product basis set are used to do the calculations. Rotational transition frequencies and rotational constants are in good agreement with experiment. We calculate states localized in both polar and nonpolar wells on the potential surface. Two of the four isotopologues we study have inequivalent monomers. They have wavefunctions localized over a single polar well.

1 Introduction

In recent years there have been several experimental[1–15] and theoretical[16–20] studies of the nitrous oxide Van der Waals dimer. The $(N_2O)_2$ potential energy surface (PES) has several accessible minima. A non-polar C_{2h} slipped anti-parallel structure was first identified and characterized.[2,5] Later, a polar form of $(N_2O)_2$ was predicted[16] and observed.[9,11,12,14]

In previous papers we reported transition frequencies and rotational constants for $(^{14}N_2O)_2$,[18,19] which agree well with experimental results. Experimentalists have also studied, $(^{15}N_2O)_2$,[11,14,17] $(^{15}N^{14}NO)_2$,[5] $^{14}N_2O–^{15}N_2O$[13,14] and $^{15}N^{14}NO–^{15}N_2O$.[14] For all of these isotopologues they have determined rotational constants for the ground vibrational state of the polar and/or nonpolar forms. Rotational constants for the torsion, geared bend, and antigeared bend states have also been reported for some of the isotopologues.[10,13,15] In this paper we compare the experimental numbers with results we obtain using the PES of ref. 18 and confirm that both the adiabatic separation of inter- and intra-molecular coordinates employed in ref. 18 and 19 and the PES of ref. 18 are accurate. According to the Born–Oppenheimer approximation, spectra for all isotopologues can be computed from one PES. It is known that for light molecules non-Born–Oppenheimer effects can shift energy levels by $\sim 1 \text{ cm}^{-1}$.[21] As the experimentalists' results for nitrous oxide dimer are very precise, it is important to know how well the Born–Oppenheimer approximation works.

Nitrous oxide dimers with equivalent monomers have two identical polar wells, and each polar wavefunction has amplitude in both polar wells. Isotopologues with different monomers are of particular interest because, although the polar wells are identical, each wavefunction has amplitude in only one of the two wells, due to the fact that there is almost no tunnelling

between the wells. The transition frequencies and rotational constants we compute could facilitate the assigning of experimentally observed transitions, help experimentalists discover transitions that have heretofore not been observed, and understand spectral patterns. See for example ref. 22.

2 Calculating rovibrational levels

The rovibrational Schrödinger equation is solved using the approach of ref. 18 and 19. The full potential can be written as a sum of an intra-molecular term, an inter-molecular term, and a coupling term. The inter-molecular term is the potential of ref. 18. We neglect the coupling term and use an adiabatic approximation to separate inter- and intra-molecular coordinates. To make the kinetic energy operator (KEO) for the effective inter-molecular Hamiltonian we use experimental constants. Three vectors: $\vec{r}_1$, $\vec{r}_2$, and $\vec{r}_0$ define the intermolecular coordinates. See Fig. 1. Vectors $\vec{r}_1$ and $\vec{r}_2$ point toward O and are aligned with the monomers. Vector $\vec{r}_0$ points from the centre of mass of monomer 1 to that of monomer 2. The four vibrational coordinates ϕ_2, θ_1, θ_2, and r_0 are defined in the standard fashion. θ_k is the angle between $\vec{r}_0$ and $\vec{r}_k$, ϕ_2 is the dihedral angle from $\vec{r}_1$ to $\vec{r}_2$ around $\vec{r}_0$; and r_0 is the length of $\vec{r}_0$. Euler angles specify the orientation of a body-fixed frame attached such that the z-axis is along $\vec{r}_0$ and the x-axis is along the vector $(\vec{r}_0 \times \vec{r}_1) \times \vec{r}_0$. The kinetic energy operator in these coordinates is well known.[23–25]

To specify the KEO, we must choose masses and monomer rotational constants. The masses used to calculate the reduced mass for the inter-monomer distance (r_0) are 14.0030740052 u,[26] 15.000108973 u,[26] and 15.9949146221 u[27] for ^{14}N, ^{15}N, and O respectively. We calculate energy levels for a particular intramolecular state of the dimer. For different intra-molecular states we use different monomer rotational constants in the
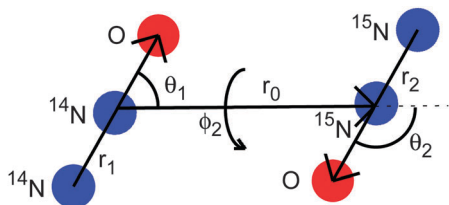
Queen's University, Kingston, Ontario K7L 3N6, Canada

This journal is © the Owner Societies 2013

Phys. Chem. Chem. Phys., 2013, **15**, 19159–19168 | **19159**

Fig. 1 $(N_2O)_2$ coordinates. O is red and N is blue.

dimer KEO. For the ground state of a dimer we use monomer rotational constants for the ground state of the monomers. For the various monomer isotopologues, they are taken from ref. 28. For excited states of dimers with different monomers we calculate energy levels for an intra-molecular dimer state with one monomer in its ground state and another excited in its $\nu_1 = 1$ state. To do these calculations we use the $\nu_1 = 1$ monomer rotational constant for $^{14}N_2O$ from ref. 28 and the $\nu_1 = 1$ monomer rotational constant for $^{15}N_2O$ from ref. 29. For dimers with identical monomers, there are two excited states: the symmetric combination (in-phase) and the anti-symmetric combination (out-of-phase). The in-phase state of the non-polar isomer is infra-red inactive because it has symmetry A_g in the C_{2h} point group. Therefore we only calculate energy levels for the out-of-phase state $(1/\sqrt{2})(||v_1^a = 1\rangle|v_1^b = 0\rangle - |v_1^a = 0\rangle|v_1^b = 1\rangle)$, where a and b label the two monomers. In this case, the appropriate rotational constant, for both monomers is $(B_0 + B_1)/2$, where B_0 is the monomer rotational constant for the ground state and B_1 is the monomer rotational constant for the $\nu_1 = 1$ state.

Energy levels and wavefunctions of a basis representation of the inter-molecular Hamiltonian are computed using a symmetry adapted Lanczos (SAL) algorithm.[30,31] Filter Diagonalization is another option.[32,33] Potential matrix elements are computed by quadrature. Matrix-vector products required to use the Lanczos algorithm are computed by evaluating sums sequentially using techniques described in ref. 25 and 34–39. Wavefunctions were obtained from the eigenvectors of the Hamiltonian matrix using methods described previously.[36,37]

Basis functions are functions of the four inter-molecular coordinates. For r_0 we use 25 potential optimized discrete variable representation (PODVR) functions[40,41] for a cut reference potential obtained by setting the other three coordinates equal to equilibrium values of the nonpolar configuration. The PODVR functions are computed in a sine basis, defined in the range [4.5 Bohr, 18.0 Bohr].[42] For the angular and rotational coordinates, we use parity adapted rovibrational functions,[36,43]

$$\left|u_{l_1 l_2 m_2; K}^{JP}\right\rangle = N_{m_2, K} \frac{1}{\sqrt{2}}\left[|l_1 l_2 m_2; JK\rangle + (-1)^{J+P}|l_1 l_2 \bar{m}_2; J\bar{K}L\rangle\right],$$
(1)

with $\bar{m}_2 = -m_2$ and $\bar{K} = -K$, and $N_{m_2, K} = \left(1 + \delta_{m_2,0}\delta_{K,0}\right)^{-1/2}$. The ket in this equation is defined by

$$\langle\theta_1, \theta_2, \phi_2; \alpha, \beta, \gamma|l_1 l_2 m_2; JK\rangle$$
$$= \sqrt{\frac{2J+1}{8\pi^2}}\Theta_{l_1}^{K-m_2}(\theta_1) Y_{l_2}^{m_2}(\theta_2, \phi_2) D_{MK}^J(\alpha, \beta, \gamma)^*$$
(2)

with

$$Y_{l_2}^{m_2}(\theta_2, \phi_2) = \frac{1}{\sqrt{2\pi}}\Theta_{l_1}^{m_2}(\theta_2)e^{im_2\phi_2}.$$
(3)

$\Theta_l^m(\theta)$ is the normalized associated Legendre function with the $(-1)^m$ Condon–Shortley phase factor, and D_{MK}^J is the Wigner function[44] of the Euler angles (α, β, γ). For more detail see ref. 18, 19 and 43. The maximum value of the indices of the bend-rotation functions, l_1, l_2, and m_2 is 44. We have previously[18] confirmed that this basis is large enough to converge levels of $(^{14}N_2O)_2$ to 0.001 cm^{-1} and assume that convergence errors for the isotopologues studied in this paper will be similar. For θ_1 and θ_2, we used 45 Gauss–Legendre quadrature points and for ϕ_2 we used 90 equally spaced trapezoid points in the range $[0,2\pi]$, with zero being the first point. Due to inversion symmetry about half of the ϕ_2 points are actually used. The size of the vibrational even-parity basis is about 628 000. A potential ceiling[34] was used to reduce the spectral range. About 82 percent of the quadrature points are below the ceiling value of 5240 cm^{-1}.

The use of the parity adapted-basis makes it possible to separately compute even and odd parity levels. For complexes with different monomers ($^{15}N^{14}NO$–$^{15}N_2O$ and $^{14}N_2O$–$^{15}N_2O$), the only symmetry operation is (space-fixed) inversion and states are labelled only by their parity: even (+) or odd (−). When the monomers are identical (($^{15}N_2O)_2$ and ($^{15}N^{14}NO)_2$) the Hamiltonian also commutes with permutation of the monomers and states are labelled (A+, B+, A−, B−) where A/B indicates whether a state is symmetric or antisymmetric with respect to permutation of the monomers. A and B states are computed separately using Symmetry Adapted Lanczos.[30,31,35]

2.1 Using the potential for other isotopologues

According to the Born–Oppenheimer approximation, the potential of ref. 18, made to compute the spectrum of $(^{14}N_2O)_2$, can be used for any isotopologue. However, the potential of ref. 18 is a function of coordinates (ϕ_2, θ_1, θ_2, and r_0) defined from Jacobi vectors that are mass-dependent. Therefore, to use the potential for other isotopologues, a coordinate transformation is required. To compute the spectrum of isotopologue b we must evaluate the potential at (quadrature and DVR) points in coordinates q^b, where q^b represents all four coordinates. We know the potential as a function of the coordinates q^a and thus require $V(q^a(q^b))$.

To obtain q^a from q^b we proceed as follows. The four coordinates ϕ_2, θ_1, θ_2, and r_0 of isotopologue b are the same as the corresponding coordinates of a virtual 4-atom molecule $(NX)_2$, where the X atom is at the centre of mass of the inner N atom and the neighbouring O atom of a monomer and the mass of X is $M_N + M_O$. We denote the lengths of the two NX bonds as r_1' and r_2'. From r_1' and r_2' and the four q^b coordinates we obtain Cartesian coordinates for the three Jacobi vectors $\vec{r}_0$, $\vec{r}_1'$, and $\vec{r}_2'$ by (arbitrarily) attaching a Cartesian axis system to the molecule. Knowing these Cartesian coordinates we can determine Cartesian components of position vectors of the atoms of the virtual molecule,

$$\Xi_i = J^{-1}\rho_i.$$
(4)

19160 | *Phys. Chem. Chem. Phys.*, 2013, **15**, 19159–19168

This journal is © the Owner Societies 2013

In this equation,

$$J^{-1} = \begin{pmatrix} \dfrac{-M_{X^2}}{M_{N^1}+M_{X^2}} & 0 & -\dfrac{M_{N^3}+M_{X^4}}{M_{N^1}+M_{X^2}+M_{N^3}+M_{X^4}} & 1 \\[2ex] \dfrac{M_{N^1}}{M_{N^1}+M_{X^2}} & 0 & -\dfrac{M_{N^3}+M_{X^4}}{M_{N^1}+M_{X^2}+M_{N^3}+M_{X^4}} & 1 \\[2ex] 0 & \dfrac{-M_{X^4}}{M_{N^3}+M_{X^4}} & \dfrac{M_{N^1}+M_{X^2}}{M_{N^1}+M_{X^2}+M_{N^3}+M_{X^4}} & 1 \\[2ex] 0 & \dfrac{M_{N^3}}{M_{N^3}+M_{X^4}} & \dfrac{M_{N^1}+M_{X^2}}{M_{N^1}+M_{X^2}+M_{N^3}+M_{X^4}} & 1 \end{pmatrix},$$

$$(5)$$

is the inverse of the matrix used to transform position vectors to Jacobi vectors, see for example ref. 25, $\rho_i = (r_{1i}{}'r_{2i}{}'r_{0i}r_{4i})^{\mathrm{T}}$, where r_{ki} is the i'th Cartesian component of Jacobi vector r_k, $k = 0$, 1, 2 and r_4 is the centre of mass vector and $\Xi_i = (N_i^1, X_i^2, N_i^3, X_i^4)^{\mathrm{T}}$. The Cartesian position vectors of isotoplogue a are then taken as equal to those of isotoplogue b. From the Cartesian position vectors of isotoplogue a we obtain Cartesian components of the Jacobi vectors for the virtual molecule associated with isotopologue a by using a J matrix. From the Cartesian components we get the Jacobi coordinates for the virtual molecule associated with isotopologue a which are equal to the Jacobi coordinates for isotopologue a.

3 Results

3.1 Energies and labels for $J = 0$

The low lying states for the isotopologues with equivalent and inequivalent monomers are shown in Tables 1 and 2 respectively. In all tables, we report four decimal places (in cm^{-1}) because the energies in the tables are relative to zero point energy (ZPE). Relative errors are little affected by non-adiabatic and non-Born–Oppenheimer effects. The labels for the states are of the form (type; ν_t (torsion), ν_g (geared bend), ν_r (VdW-stretch), ν_a (anti-geared bend)), where type is the well above which the wavefunction is localized. N is the label for the nonpolar well and P is the label for the polar wells. When the monomers are equivalent, polar levels are split by less than 0.0001 cm^{-1} and polar wavefunctions have amplitude in both polar wells. Previous calculations[19] demonstrated this for $(^{14}N_2O)_2$, and in this paper we show that it is also true for $(^{15}N_2O)_2$.

To label the $J = 0$ states, probability density (PD) plots were made by integrating over all but two coordinates. The PDs are normalized with a volume element with a $\sin\theta$ factor for each θ angle and an r_0^2 factor for r_0. The only wavefunctions we examined that are localized above more than one well are those for polar states of dimers with identical monomers. It is thus easy to identify the ground state for each type. The $\nu_t = 1$, $\nu_g = 1$, $\nu_r = 1$, and $\nu_a = 1$ fundamentals can be labelled on the basis of the nodal structure of the PDs. Four single-node wavefunctions were observed. PDs for the $\nu_r = 2$ stretch and $\nu_a = 1$ anti-gear fundamental are shown in Fig. 2. For some combination and overtone states, it was not possible to label using only PDs. In these cases, energies of the fundamentals were also used.

The energy of the $(^{15}N_2O)_2$ state with $E + 64.7030\ \mathrm{cm}^{-1}$, assigned to (N;1100), is approximately the sum of the energy of the $\nu_t = 1$ state ($\approx 25.4\ \mathrm{cm}^{-1}$) and the energy of the $\nu_g = 1$ state ($\approx 41.3\ \mathrm{cm}^{-1}$). The strategy of using fundamental energies to guide the assignment is more important when labelling the anti-gear and VdW stretch combinations and overtones because the corresponding PDs are more complicated due to coupling.[18,19]

Our fundamental energies can be compared with experimental counterparts. A torsion band was observed for $(^{14}N_2O)_2$ in 2009.[17] Very recently the same band has been discovered for $(^{15}N_2O)_2$.[15] For $(^{14}N_2O)_2$, the experimental torsion frequency, 27.3(1.0) cm^{-1}, is close to the theoretical value, 25.7599 cm^{-1}, of ref. 18. For $(^{15}N_2O)_2$, the experimental frequency is 26.9(1.0) cm^{-1} and we find (Table 1) 25.3644 cm^{-1}. Although for both isotopologues, the calculated and experimental frequencies are not equal, the difference in the torsion frequency between the two isotopologues is 0.4 cm^{-1}, for both experiment and theory. For the geared (disrotatory) bend fundamental, the $(^{14}N_2O)_2$ frequency is 42.3(1.0) cm^{-1} (ref. 13 and 17) and the calculated value is 41.8609 cm^{-1}. For $(^{15}N_2O)_2$, the experimental value is 41.6(1.0) cm^{-1} and we compute 41.2860 cm^{-1}. In this case, the the experimental and calculated frequencies do agree to within experimental error. According to experiment, the geared frequencies of the two isotopologues differ by $-0.7\ \mathrm{cm}^{-1}$; according to our calculation the difference is $-0.6\ \mathrm{cm}^{-1}$. Recently, the anti-gear fundamental was observed at 96.0926 cm^{-1} and 95.4913 cm^{-1} for $(^{14}N_2O)_2$ and $(^{15}N_2O)_2$ respectively.[15] The calculated values are 97.5221 cm^{-1} and 97.0473 cm^{-1}. Once again, the theoretical calculations and experimental measurements have similar frequency shifts ($-0.5\ \mathrm{cm}^{-1}$ and $-0.6\ \mathrm{cm}^{-1}$).

In ref. 14 the monomer with an N inside is denoted A and the monomer with an N outside is denoted B. When the monomers are not equivalent, notation is required to distinguish the two wells and their associated states. In this work, a dimer for which monomer A is lighter is called P_A and a dimer for which monomer B is lighter is called P_B. For $^{14}N_2O$–$^{15}N_2O$, the dimer denoted by $N_{(A,1)}N_{(A,2)}$ in ref. 14 is called P_A in this work. For $^{15}N^{14}NO$–$^{15}N_2O$, the dimer denoted by $N_{(A,2)}$ in ref. 14 is called P_A in this work. See Fig. 3 and 4 for illustrations. For dimer X–Y, r_1 and θ_1 are coordinates of monomer X and r_2 and θ_2 are coordinates of monomer Y. In order to assign the wavefunctions to either P_A or P_B, we look at probability density (PD) plots. Wavefunctions with amplitude in the P_A well have $\theta_1 > 90°$ and $\theta_2 > 90°$, as is shown in Fig. 3.

For isotopologues with different monomers, although the two polar wells have the same shape and depth, vibrational wavefunctions are localized in only one polar well. See Fig. 3 for plots of probability density for the $^{14}N_2O$–$^{15}N_2O$. The energy of the P_A vibrational state is higher than the energy of the P_B vibrational state. For $^{15}N^{14}NO$–$^{15}N_2O$, plots of probability density of P_A and P_B states are shown in Fig. 4. Also in this case, the vibrational energy of the P_A state is higher, however, the difference between the P_A and P_B energies (0.015 cm^{-1}) is much smaller than the $^{14}N_2O$–$^{15}N_2O$ difference (0.386 cm^{-1}), presumably due to the smaller difference between the monomer masses. The order of the P_A and P_B vibrational energies for

This journal is © the Owner Societies 2013

Phys. Chem. Chem. Phys., 2013, **15**, 19159–19168 | **19161**

Table 1 The lowest vibrational levels (in cm^{-1}) of (^{15}N$_2$O)$_2$ and (^{15}N^{14}NO)$_2$ for each irrep. relative to the ZPE. The quantum numbers v_t (torsion), v_g (geared bend), v_r (VdW-stretch), v_a (anti-geared bend) are for the four intermolecular modes. The labels are (well; v_t, v_g, v_r, v_a). The ZPE of (^{15}N$_2$O)$_2$ and (^{15}N^{14}NO)$_2$ are −515.9024 and −515.4559, respectively

A+	B+	A−	B−
(^{15}N$_2$O)$_2$			
0.0000(N;0000)	41.2860(N;0100)	25.3644(N;1000)	64.7030(N;1100)
49.9506(N;2000)	85.4353(N;0110)	73.3442(N;3000)	108.2692(N;1110)
51.6079(N;0010)	89.0123(N;2100)	75.8042(N;1010)	112.2575(N;3100)
79.2953(N;0200)	112.5860(N;0300)	102.5049(N;1200)	136.6005(N;1300)
96.3946(N;4000)	126.6917(N;0120)	119.2646(N;5000)	149.5334(N;1120)
97.0473(N;0001)	130.9050(N;2110)	120.2643(N;1001)	152.3685(N;3110)
99.2091(N;0020)	134.2485(N;0101)	122.4350(N;3010)	156.2541(N;1101)
100.0734(N;2010)	135.3983(N;4100)	123.0847(N;1020)	157.4220(N;5100)
114.9930(N;0210)	141.8673(N;0310)	139.1094(N;1210)	164.7427(P;1000)
126.0668(N;2200)	143.6184(P;0000)	148.1570(N;3200)	
138.5227(N;0400)		162.0301(N;1220)	
141.4709(N;6000)		162.3369(N;7000)	
142.4823(N;2001)		164.3517(N;5010)	
143.4326(N;0011)		164.7427(P;1000)	
143.6184(P;0000)			
145.0899(N;4010)			
(^{15}N^{14}NO)$_2$			
0.0000(N;0000)	41.2680(N;0100)	25.3588(N;1000)	64.6846(N;1100)
49.9675(N;2000)	85.7062(N;0110)	73.3787(N;3000)	108.5322(N;1110)
52.0146(N;0010)	89.0003(N;2100)	76.1595(N;1010)	112.2495(N;3100)
79.3263(N;0200)	112.7371(N;0300)	102.5525(N;1200)	136.7507(N;1300)
96.4881(N;4000)	126.9851(N;0120)	119.3375(N;5000)	149.8323(N;1120)
97.2825(N;0001)	131.1331(N;2110)	120.5656(N;1001)	152.6032(N;3110)
99.7066(N;2010)	134.3627(N;4100)	122.7463(N;3010)	156.3860(N;1101)
100.5825(N)	135.5489(N;2110)	123.6696(N;1020)	157.5508(N;5100)
115.2980(N;0210)	142.2876(N;0310)	139.4306(N;1210)	164.6524(P;1000)
126.1184(N;2200)	143.5421(P;0000)	148.2189(N;3200)	
138.8338(N;0400)		162.3374(N;1220)	
141.5690(N;6000)		162.4907(N;1400)	
142.8702(N;2001)		164.6059(N;5010)	
143.5421(P;0000)		164.6524(P;1000)	
143.9925(N;2020)			
145.3756(N;4010)			

the dimers with inequivalent monomers, predicted by our calculations, has not been confirmed by the experiment. This could perhaps be done in the infrared. Of course, the energy of the polar isomers of the dimers with equivalent monomers studied in this work have not been measured either.

3.2 $J > 0$ energy levels and rotational constants for ground and fundamentals

$J > 0$ levels have also been calculated for each isotopologue. The $J = 1$ energies and rotational constants, for nonpolar and polar levels are shown in Tables 3 and 4 respectively. Where possible, comparisons have been made to experimental rotational constants. These are the italicized numbers in the tables. The experimentalists determine rotational constants by adjusting the parameters of an effective rotational Hamiltonian so that its eigenvalues reproduce rotational energy levels consistent with transitions associated with a particular vibrational state. With the definition that monomer A has an N on the inside and monomer B has an N on the outside, as indicated in Fig. 3 of ref. 14, columns 2 and 3 and also columns 4 and 5 of ref. 14 must be permuted.[45] Rotational constants we report are obtained directly from the $J = 1$ levels we compute by assigning them to vibrational states.

To assign ro-vibrational levels to vibrational states we use the two methods described in ref. 19. The first uses line strengths calculated from a sum-of-dipoles model for the dipole moment of (N$_2$O)$_2$. Equations for computing the line strengths are given in ref. 19 If vibrational states were widely spaced it would be easy to assign ro-vibrational levels to vibrational states. This is not the case for the nitrous oxide dimer. However, vibrational states localized above polar wells *are* widely spaced and therefore if we can extract the ro-vibrational levels associated with polar vibrational states from the full list of ro-vibrational levels they can be attributed to vibrational states by using previously established assignments of $J = 0$ energy levels. This is successful, even if the polar states are embedded in a region with many nonpolar (dark) energies. $R(0)$ transitions that are intense must be to $J = 1$ states of polar vibrational states. As the dipole moment is in the plane perpendicular to the c-axis, only a-type and b-type transitions will be bright. The $R(0)$ transitions are therefore to 1_{01} and 1_{11} states only. 1_{10} states can be identified by computing $Q(1)$ transition line strengths. Fig. 11 of ref. 19 illustrates these transitions. A list of the bright $R(0)$ and $Q(1)$ transition frequencies and their line strengths for (P;0000) is in Table 7.

Using line strengths it is not possible to assign nonpolar states nor is it possible for polar states of dimers with equivalent
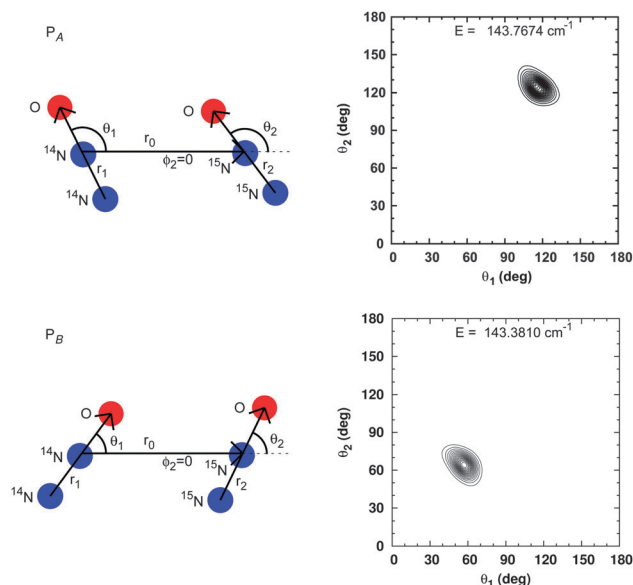
Table 2 The lowest vibrational levels relative to the ZPE, (in cm^{-1}) of $^{14}N_2O$–$^{15}N_2O$ and $^{15}N^{14}NO$–$^{15}N_2O$ for each irrep. The quantum numbers v_t (torsion), v_g (geared bend), v_r (VdW-stretch), v_a (anti-geared bend) are for the four intermolecular modes. Labels are (well; v_t, v_g, v_r, v_a). The ZPE of $^{14}N_2O$–$^{15}N_2O$ and $^{15}N^{14}NO$–$^{15}N_2O$ are −515.0549 and −515.6788, respectively

$^{14}N_2O$–$^{15}N_2O$		$^{15}N^{14}NO$–$^{15}N_2O$	
+	−	+	−
0.0000(N;0000)	25.5633(N;1000)	0.0000(N;0000)	25.3616(N;1000)
41.5625(N;0100)	65.1640(N;1100)	41.2770(N;0100)	64.6939(N;1100)
50.3632(N;2000)	73.9630(N;2000)	49.9607(N;2000)	73.3634(N;3000)
52.1940(N;0010)	76.5353(N;1010)	51.8109(N;0010)	75.9811(N;1010)
79.8406(N;0200)	103.2530(N;1200)	79.3109(N;0200)	102.5288(N;1200)
86.1021(N;0110)	109.1243(N;1110)	85.5722(N;0110)	108.4023(N;1110)
89.6636(N;2100)	113.0796(N;3100)	89.0062(N;2100)	112.2532(N;3100)
97.0881(N;4000)	120.2768(N;5000)	96.4496(N;0001)	119.3078(N;5000)
97.5102(N;2010)	120.9475(N;1001)	97.1600(N;2010)	120.4127(N;1001)
100.1038(N;0001)	123.2829(N;3010)	99.4651(N;4000)	122.5906(N;3010)
101.0014(N;0020)	124.1754(N;1020)	100.3217(N;0020)	123.3769(N;1020)
113.2866(N;0300)	137.4908(N;1300)	112.6620(N;0300)	136.6762(N;1300)
115.8601(N;0210)	140.1793(N;1210)	115.1456(N;0210)	139.2704(N;1210)
126.9682(N;2200)	149.1896(N;3200)	126.0928(N;2200)	148.1881(N;3200)
127.5887(N;0120)	150.6165	126.8406(N;0120)	149.6858
131.8691(N;2110)	153.4795(N;3110)	131.0207(N;2110)	152.4866(N;3110)
134.8914(N;0101)	157.9916(N;1110)	134.3082(N;0101)	156.3220(N;1101)
136.2645(N;4100)	158.5032(N;5100)	135.4704(N;4100)	157.4839(N;5100)
139.3557(N;0400)	163.0892(N;1220)	138.6809(N;0400)	162.1979
142.6543(N;6000)	163.5930(N;7000)	141.5287(N;6000)	162.4099(N;7000)
142.8754(N;0301)	164.6521(P$_B$;1000)	142.0781(N;0301)	164.4812(N;5010)
143.3810(P$_B$;0000)	165.0188(P$_A$;1000)	142.6808(N;4100)	164.6898(P$_B$;1000)
143.4422(N;4100)	165.4287(N;5010)	143.5725(P$_B$;0000)	164.7056(P$_A$;1000)
143.7674(P$_A$;0000)	166.4179	143.5882(P$_A$;0000)	165.5514
144.3883(N;2001)	166.6013	143.7067(N;2001)	165.6570
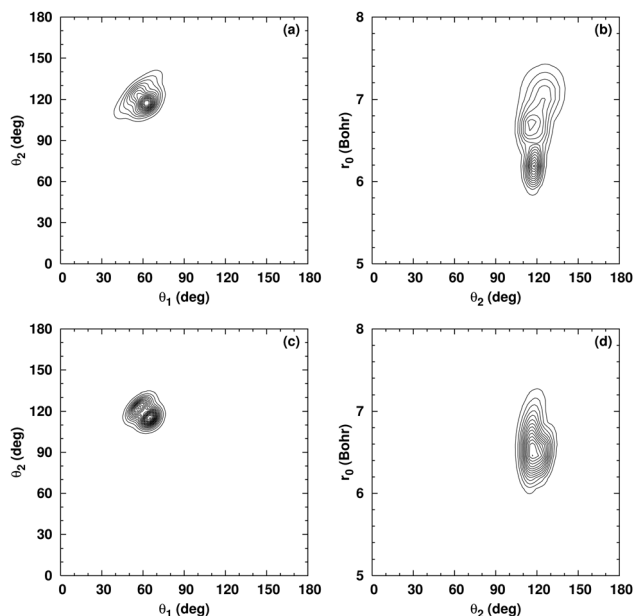
**Fig. 2** PD plots of the (N;0020)[(a) and (b)] at 99.2091 cm^{-1}, and (N;0001)[(c) and (d)] at 97.0473 cm^{-1} states for the $(^{15}N_2O)_2$ isotopologue. There is clear coupling between the coordinates so the use of fundamental energies to guide assignment becomes important.

Fig. 3 Polar equilibrium geometries and probability densities for the $^{14}N_2O$–$^{15}N_2O$ complex.

monomers to identify which of the two tunnelling states should be assigned to a polar ro-vibrational state participating in a bright transition (for the dimers with non-equivalent monomers, ro-vibrational states can be assigned to one of the two tunnelling states of the polar isomer, due to their splitting). Both of these deficiencies of the line-strength method can be rectified by using the second method of ref. 19, called vibrational parent analysis (VPA). Using VPA we also confirm the assignments from the intensity analysis. To do VPA, the calculated rovibrational wavefunctions are expanded in terms of vibrational wavefunctions.[19,46]
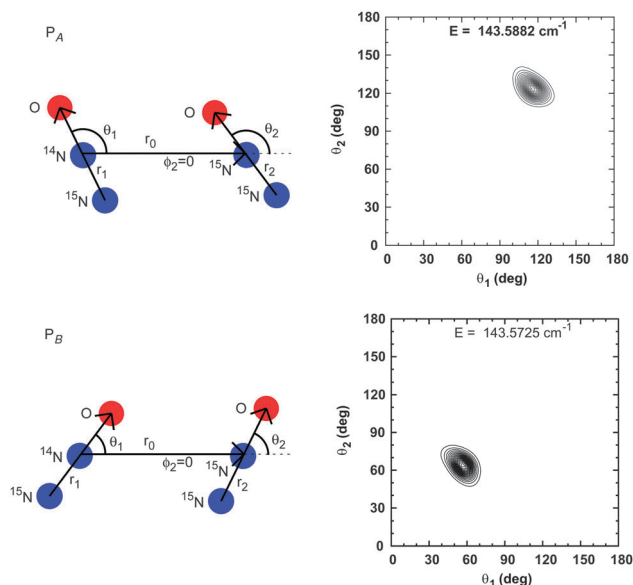
Fig. 4   Polar equilibrium geometries and probability densities for the $^{15}N^{14}NO$–$^{15}N_2O$ complex.

Once one has assigned a vibrational label (with a known symmetry) to a rovibrational state (also of known symmetry) it is possible, to determine the symmetry of the rotational function, using the product rule, $\Gamma_{vr} = \Gamma_v\Gamma_r$. For states localized in the nonpolar well, the symmetries of the 1_{01}, 1_{11}, and 1_{10} rotational functions are B−, B−, and A+ respectively. This is

denoted case a in ref. 19. For polar states, the symmetries are B−, A−, and B+ which is denoted case b. In ref. 19, the bright transitions occur both within and across a tunnelling pair. When the monomers are not equivalent, the exchange symmetry is broken and there are two distinct polar states (as shown in Fig. 3). In this case bright transitions occur only among states associated with one of the polar wells. The 1_{01}, 1_{11}, and 1_{10} rotational functions have symmetries −, −, and + for states localized above either well. For the nonpolar well, the rotational functions are also −, −, and +.

For the ground nonpolar state, computed rotational constants can be compared to experimental values for $(^{15}N_2O)_2$, $(^{15}N^{14}NO)_2$ and $^{14}N_2O$–$^{15}N_2O$. The discrepancy between the theoretical and fitted experimental values is similar for all isotopologues. The A rotational constants differ by between 0.0012 and 0.0013 cm^{-1}, the calculated and observed B constants are equal (to within the number of digits we report), and the C constants differ by <0.0001 cm^{-1}. These differences are all close to those reported in ref. 18. The nonpolar ground state rotational constants for $^{14}N_2O$–$^{15}N_2O$ of ref. 17, computed from the geometry of the nonpolar configuration on their PES are $A = 0.2943$ cm^{-1}, $B = 0.06058$ cm^{-1}, and $C = 0.05024$ cm^{-1}. They are considerably further from the experimental values than are the results in Table 3.

For the ground polar state, the discrepancy between experiment and theory is larger for some isotopologues than for others. For the equivalent-monomer isotopologue $(^{15}N_2O)_2$, the theory–expt differences are -0.0009 cm^{-1}, $+0.0003$ cm^{-1}, and $+0.0002$ cm^{-1}

Table 3 $J = 1$ rotational levels and rotational constants (in cm^{-1}) for the nonpolar ground and fundamental states of each isotopologue. Experimental numbers are in italics

$J = 0$ (W; v_t, v_g, v_r, v_a) (sym)	1_{01} (sym)	1_{11} (sym)	1_{10} (sym)	A	B	C
$(^{15}N_2O)_2$						
0.0000(N;0000)(A+)	0.1036(B−)	0.3424(B−)	0.3515(A+)	0.2952	0.0564	0.0473
$(N;0000)^{11}$				0.2940	0.0564	0.0472
25.3645(N;1000)(A−)	25.4680(B+)	25.6966(B+)	25.7051(A−)	0.2846	0.0560	0.0475
41.2860(N;0100)(B+)	41.3873(A−)	41.6414(A−)	41.6504(B+)	0.3092	0.0552	0.0462
51.6079(N;0010)(A+)	51.7089(B−)	51.9543(B−)	51.9630(A+)	0.3003	0.0548	0.0461
97.0473(N;0001)(A+)	97.1496(B−)	97.3778(B−)	97.3863(A+)	0.2836	0.0554	0.0469
$(^{15}N^{14}NO)_2$						
0.0000(N;0000)(A+)	0.1056(B−)	0.3437(B−)	0.3532(A+)	0.2957	0.0575	0.0481
$(N;0000)^{5}$				0.2944	0.0575	0.0480
25.3588(N;1000)(A−)	25.4643(B+)	25.6921(B+)	25.7009(A−)	0.2850	0.0571	0.0483
41.2680(N;0100)(B+)	41.3713(A−)	41.6248(A−)	41.6342(B+)	0.3098	0.0563	0.0470
52.0146(N;0010)(A+)	52.1173(B−)	52.3624(B−)	52.3714(A+)	0.3009	0.0559	0.0469
97.2825(N;0001)(A+)	97.3865(B−)	97.6172(B−)	97.6263(A+)	0.2873	0.0566	0.0474
$^{14}N_2O$–$^{15}N_2O$						
0.0000(N;0000)(+)	0.1067(−)	0.3463(−)	0.3559(+)	0.2978	0.0581	0.0485
$(N;0000)^{13}$				0.2966	0.0581	0.0485
25.5633(N;1000)(−)	25.6698(+)	25.8993(+)	25.9082(−)	0.2872	0.0577	0.0488
41.5624(N;0100)(+)	41.6668(−)	41.9219(−)	41.9314(+)	0.3120	0.0569	0.0474
52.1940(N;0010)(+)	52.2978(−)	52.5445(−)	52.5536(+)	0.3032	0.0564	0.0474
100.1038(N;0001)(+)	100.2049(−)	100.4258(−)	100.4329(+)	0.2750	0.0542	0.0470
$^{15}N^{14}NO$–$^{15}N_2O$						
0.0000(N;0000)(+)	0.1046(−)	0.3431(−)	0.3524(+)	0.2954	0.0570	0.0477
25.3616(N;1000)(−)	25.4661(+)	25.6943(+)	25.7030(−)	0.2848	0.0566	0.0479
41.2770(N;0100)(+)	41.3793(−)	41.6331(−)	41.6423(+)	0.3095	0.0558	0.0466
51.8109(N;0010)(+)	51.9127(−)	52.1581(−)	52.1669(+)	0.3006	0.0553	0.0465
96.4496(N;0001)(+)	96.5530(−)	96.7582(−)	96.7650(+)	0.2603	0.0551	0.0483

Table 4 $J = 1$ rotational levels and rotational constants (in cm^{-1}) for the npolar ground and fundamental states of each isotopologue. Experimental numbers are in italics

$J = 0$ (W; ν_t, ν_g, ν_r, ν_a) (sym)	1_{01} (sym)	1_{11} (sym)	1_{10} (sym)	A	B	C
$(^{15}N_2O)_2$						
143.6184(P;0000)(A+)	143.7147(B−)	143.9598(A−)	143.9677(B+)	0.2972	0.0521	0.0442
143.6184(P;0000)(B+)	143.7147(A−)	143.9598(B−)	143.9677(A+)	0.2972	0.0521	0.0442
$(P;0000)^{11,14}$				0.2981	*0.0518*	*0.0440*
164.7427(P;1000)(A−)	164.8430(B+)	165.1925(A+)	165.2010(B−)	0.4039	0.0544	0.0459
164.7427(P;1000)(B−)	164.8430(A+)	165.1925(B+)	165.2010(A−)	0.4039	0.0544	0.0459
$(^{15}N^{14}NO)_2$						
143.5421(P;0000)(A+)	143.6402(B−)	143.8849(A−)	143.8931(B+)	0.2979	0.0531	0.0450
143.5421(P;0000)(B+)	143.6402(A−)	143.8849(B−)	143.8931(A+)	0.2979	0.0531	0.0450
164.6524(P;1000)(A−)	164.7546(B+)	165.1047(A+)	165.1135(B−)	0.4056	0.0555	0.0467
164.6524(P;1000)(B−)	164.7546(A+)	165.1047(B+)	165.1135(A−)	0.4056	0.0555	0.0467
$^{14}N_2O$–$^{15}N_2O$						
143.3811(P$_B$;0000)(+)	143.4802(−)	143.7262(−)	143.7345(+)	0.2997	0.0537	0.0454
$(P_A;0000)^{14}$				*0.3006*	*0.0534*	*0.0453*
143.7674(P$_A$;0000)(+)	143.8651(−)	144.1180(−)	144.1260(+)	0.3058	0.0528	0.0449
$(P_B;0000)^{14}$				*0.3065*	*0.0524*	*0.0447*
164.6521(P$_B$;1000)(−)	164.7554(+)	165.1029(+)	165.1120(−)	0.4037	0.0562	0.0471
165.0188(P$_A$;1000)(−)	165.1204(+)	165.4833(+)	165.4918(−)	0.4180	0.0550	0.0466
$^{15}N^{14}NO$–$^{15}N_2O$						
143.5725(P$_B$;0000)(+)	143.6698(−)	143.9146(−)	143.9226(+)	0.2975	0.0526	0.0446
$(P_A;0000)^{14}$				*0.2983*	*0.0524*	*0.0444*
143.5882(P$_A$;0000)(+)	143.6854(−)	143.9304(−)	143.9385(+)	0.2977	0.0526	0.0446
$(P_B;0000)^{14}$				*0.2985*	*0.0523*	*0.0444*
164.6898(P$_B$;1000)(−)	164.7911(+)	165.1408(+)	165.1494(−)	0.4046	0.0549	0.0463
164.7056(P$_A$;1000)(−)	164.8068(+)	165.1567(+)	165.1653(−)	0.4049	0.0549	0.0463

for A, B, C, respectively. The same differences are reported for $(^{14}N_2O)_2$ in ref. 19. Similar differences are obtained for $^{15}N^{14}NO$–$^{15}N_2O$ and P$_A$ of $^{14}N_2O$–$^{15}N_2O$. P$_B$ of $^{14}N_2O$–$^{15}N_2O$ has differences of -0.0007 cm^{-1}, $+0.0004$ cm^{-1}, and $+0.0002$. Berner *et al.* also computed rotational constants from equilibrium geometries of the polar $^{14}N_2O$–$^{15}N_2O$. However, they failed to notice that columns 2 and 3 and also columns 4 and 5 of Table 2 of ref. 14 must be permuted.

Ref. 14 reports some observed polar transitions for several isotopologues and Table 5 shows the comparison between the calculated and observed transition frequencies along with line strengths calculated using the method of ref. 19. For $(^{15}N_2O)_2$, all lines with $J < 3$ are compared. The difference between the calculated and observed transitions frequencies is fairly constant for all observed transitions.

Results for the case when one of the monomers is in an excited state are shown in Table 6 for the ground and fundamental states of $^{14}N_2O$–$^{15}N_2O$. In these calculations, the monomer in the excited state with $\nu_1 = 1$ is $^{14}N_2O$. The calculated rotational constants for the (N;0000) state differ from the experimental values by 0.0015, 0.0001, and 0.0001 cm^{-1} for A, B, and C respectively. These differences are slightly larger than the differences between calculated and experimental values for the case when both monomers are not excited when they are 0.0012, 0.0000, and 0.0001 cm^{-1}.

For the $(^{15}N_2O)_2$ complex, non-polar levels and rotational constants, for the out-of-phase $\nu_1 = 1$ state, are also shown in Table 6. There are results for the ground state, and for torsion, geared and anti-geared fundamentals. Experimentally, only transitions to the

Table 5 Comparison between calculated (ν_{cal}) and observed (ν_{obs}) transition frequencies in the supplementary data of ref. 14. Calculated intensities (S) are also shown

Polar $J_{K_a''K_c''}'' \to J_{K_a'K_c'}'$	ν_{cal}(cm^{-1})	ν_{obs}(cm^{-1})	$\nu_{cal} - \nu_{obs}$(cm^{-1})	S
$(^{15}N_2O)_2$				
$1_{10} \to 1_{01}$	0.2530	0.2541	−0.0011	3.68
$0_{00} \to 1_{11}$	0.3414	0.3421	−0.0007	2.45
$2_{12} \to 1_{11}$	0.1847	0.1838	0.0009	2.16
$2_{02} \to 1_{01}$	0.1924	0.1914	0.0010	2.88
$2_{11} \to 1_{10}$	0.2005	0.1994	0.0011	2.16
$2_{11} \to 2_{02}$	0.2611	0.2621	−0.0010	6.04
$2_{12} \to 1_{01}$	0.4298	0.4301	−0.0003	3.68
$3_{13} \to 2_{12}$	0.2756	0.2769	−0.0013	3.84
$3_{03} \to 2_{02}$	0.2867	0.2881	−0.0014	4.32
$3_{12} \to 2_{11}$	0.2990	0.3007	−0.0017	4.32
$3_{12} \to 3_{03}$	0.2744	0.2736	0.0007	8.25
$^{14}N_2O$–$^{15}N_2O$				
B $0_{00} \to 1_{11}$	0.3451	0.3453	−0.0002	2.47
A $0_{00} \to 1_{11}$	0.3506	0.3512	−0.0006	2.43
$^{15}N^{14}NO$–$^{15}N_2O$				
B $0_{00} \to 1_{11}$	0.3421	0.3427	−0.0007	2.45
A $0_{00} \to 1_{11}$	0.3422	0.3429	−0.0007	2.45
B $1_{10} \to 1_{01}$	0.2529	0.2539	−0.0011	3.67
A $1_{10} \to 1_{01}$	0.2531	0.2542	−0.0011	3.67
B $1_{01} \to 2_{12}$	0.4312	0.4315	−0.0003	3.67
A $1_{01} \to 2_{12}$	0.4314	0.4317	−0.0003	3.67
B $2_{02} \to 3_{03}$	0.2909	0.2894	0.0015	4.34
A $2_{02} \to 3_{03}$	0.2907	0.2892	0.0015	4.35
B $3_{03} \to 4_{04}$	0.3869	0.3850	−0.0019	5.79
A $3_{03} \to 4_{04}$	0.3867	0.3847	−0.0020	5.79

out-of-phase $\nu_1 = 1$ band are observed because the in-phase band is infrared inactive. The (N;0000) rotational constants differ from

Table 6 $J = 1$ rotational levels and rotational constants (in cm^{-1}) for the upper ($\nu_1 = 1$) state for the ($^{15}N_2O)_2$ and $^{14}N_2O$–$^{15}N_2O$ (the light monomer is excited) isotopologues

$J = 0$ (W; ν_t, ν_g, ν_r, ν_a) (sym)	1_{01} (sym)	1_{11} (sym)	1_{10} (sym)	A	B	C
($^{15}N_2O)_2$						
0.0000(N;0000)(A+)	0.1036(B−)	0.3418(B−)	0.3510(A+)	0.2946	0.0563	0.0472
(N;0000)[13]				0.2937	0.0562	0.0471
25.3399(N;1000)(A−)	25.4434(B+)	25.6714(B+)	25.6799(A−)	0.2840	0.0560	0.0475
(N;1000)[15]				0.2812	0.0561	0.0474
41.2497(N;0100)(B+)	41.3511(A−)	41.6045(A−)	41.6136(B+)	0.3086	0.0552	0.0461
(N;0100)[13]				0.3061	0.0553	0.0461
51.6015(N;0010)(A+)	51.7024(B−)	51.9473(B−)	51.9560(A+)	0.2997	0.0548	0.0461
96.9822(N;0001)(A+)	97.0844(B−)	97.3126(B−)	97.3212(A+)	0.2836	0.0554	0.0468
(N;0001)[15]				0.2874	0.0551	0.0462
143.6359(P;0000)(A+)	143.7322(B−)	143.9768(A−)	143.9847(B+)	0.2967	0.0521	0.0442
143.6359(P;0000)(B+)	143.7322(A−)	143.9768(B−)	143.9847(A+)	0.2967	0.0521	0.0442
(P;0000)[11,12] ^{a}				0.2970	0.0517	0.0439
(P;0000)[17] ^{b}				0.2955	0.0519	0.0440
164.7414(P;1000)(A−)	164.8416(B+)	165.1907(A+)	165.1992(B−)	0.4034	0.0544	0.0459
164.7414(P;1000)(B−)	164.8416(A+)	165.1907(B+)	165.1992(A−)	0.4034	0.0544	0.0459
$^{14}N_2O$–$^{15}N_2O$						
0.0000(N;0000)(+)	0.1066(−)	0.3458(−)	0.3554(+)	0.2973	0.0581	0.0485
(N;0000)[13]				0.2958	0.0580	0.0484
25.5633(N;1000)(−)	25.6448(+)	25.8738(+)	25.8827(−)	0.2867	0.0577	0.0488
41.5275(N;0100)(+)	41.6318(−)	41.8863(−)	41.8959(+)	0.3114	0.0569	0.0474
52.1881(N;0010)(+)	52.2919(−)	52.5381(−)	52.5471(+)	0.3026	0.0564	0.0473
100.0692(N;0001)(+)	100.1704(−)	100.3899(−)	100.3970(+)	0.2736	0.0541	0.0470
143.3966(P$_B$;0000)(+)	143.4957(−)	143.7412(−)	143.7496(+)	0.2992	0.0537	0.0454
143.7866(P$_A$;0000)(+)	143.8863(−)	144.1386(−)	144.1465(+)	0.3051	0.0528	0.0449
164.6470(P$_B$;1000)(−)	164.7503(+)	165.0978(+)	165.1068(−)	0.4037	0.0561	0.0471
165.0220(P$_A$;1000)(−)	165.1236(+)	165.4857(+)	165.4941(−)	0.4171	0.0550	0.0466

^{a} The in-phase $\nu_1 = 1$ polar from ref. 11. ^{b} The out-of-phase $\nu_1 = 1$ polar from ref. 17.

Table 7 All $R(0)$ and $Q(1)$ transitions for (P;0000) with computed line strengths (S)

Polar	$J_{K_a''K_c''}'' \rightarrow J_{K_a'K_c'}'$	ν_{cal}(cm^{-1})	S
($^{15}N_2O)_2$			
	$0_{00} \rightarrow 1_{01}$	0.0963	1.44
	$0_{00} \rightarrow 1_{11}$	0.3414	2.45
	$1_{10} \rightarrow 1_{01}$	0.2531	3.68
	$1_{10} \rightarrow 1_{11}$	0.0079	2.16
($^{15}N^{14}NO)_2$			
	$0_{00} \rightarrow 1_{01}$	0.0963	1.44
	$0_{00} \rightarrow 1_{11}$	0.3414	2.45
	$1_{10} \rightarrow 1_{01}$	0.2531	3.68
	$1_{10} \rightarrow 1_{11}$	0.0079	2.16
$^{14}N_2O$–$^{15}N_2O$			
B	$0_{00} \rightarrow 1_{01}$	0.0992	1.42
A	$0_{00} \rightarrow 1_{01}$	0.0977	1.47
B	$0_{00} \rightarrow 1_{11}$	0.3451	2.47
A	$0_{00} \rightarrow 1_{11}$	0.3506	2.43
B	$1_{10} \rightarrow 1_{01}$	0.2543	3.71
A	$1_{10} \rightarrow 1_{01}$	0.2608	3.64
B	$1_{10} \rightarrow 1_{11}$	0.0083	2.13
A	$1_{10} \rightarrow 1_{11}$	0.0079	2.20
$^{15}N^{14}NO$–$^{15}N_2O$			
B	$0_{00} \rightarrow 1_{01}$	0.0972	1.45
A	$0_{00} \rightarrow 1_{01}$	0.0972	1.45
B	$0_{00} \rightarrow 1_{11}$	0.3421	2.45
A	$0_{00} \rightarrow 1_{11}$	0.3422	2.45
B	$1_{10} \rightarrow 1_{01}$	0.2529	3.67
A	$1_{10} \rightarrow 1_{01}$	0.2531	3.67
B	$1_{10} \rightarrow 1_{11}$	0.0081	2.17
A	$1_{10} \rightarrow 1_{11}$	0.0080	2.17

their experimental counterparts by 0.0009, 0.0001, and 0.0001 cm^{-1} for A, B, and C respectively. Compared to the $\nu_1 = 0$ (N;0000) state, the A constant is slightly closer to and the B constant is slightly further from the experimental value while the difference is the same for the C constant. For the (N;1000) state, the theory–expt differences are 0.0028, −0.0001, and 0.0001 cm^{-1} for A, B, and C respectively. While the B and C constants are still close to experiment, the difference in the A constant is about three times as large as for (N;0000) state. For the geared (N;0100) excited monomer state, the theory–expt differences are 0.0025, −0.0001, and 0.0000 cm^{-1} for A, B, and C respectively. Once again, the A constant is significantly over-estimated in our calculations. For the anti-gear (N;0001) state, the theory–expt differences are −0.0038, 0.0003, and 0.0006 cm^{-1} for A, B, and C respectively. These differences are larger than for any other state. The larger differences might be due in part to the fact that the fit of the experimental levels to eigenvalues of the standard rotational Hamiltonian is not as good. The order of magnitude of the error on the fitted constants for energy levels of $J < 2$ is about two orders of magnitude larger than for the other states. A possible explanation for this is coupling with the (N;0010) or (N;0020) states. The coupling with the (N;0010) state is shown in Fig. 9 of ref. 19 and the coupling with (N;0020) is shown in Fig. 2.

For the nonpolar isomer, only the in-phase monomer stretching vibration is infrared inactive. This differs from the polar isomer which has two bands, for both the in-phase and out-of-phase

19166 | Phys. Chem. Chem. Phys., 2013, **15**, 19159–19168

This journal is © the Owner Societies 2013

$\nu_1 = 1$ upper states.[17] With the adiabatic approximation we use, out-of-phase and in-phase upper states have identical energies. However, from experimental results in Table 6, a noticeable difference in the rotational constants is observed. The theory–expt difference is -0.0003, 0.0004, and 0.0003 cm^{-1} for the in-phase, and 0.0012, 0.0002, 0.0002 cm^{-1} for the out-of-phase constants A, B, and C respectively. This compares to the $\nu_1 = 0$ differences of -0.0009, 0.0003, 0.0002 cm^{-1}.

4 Conclusion

Ro-vibrational energy levels and line strengths have been computed for four isotopologues of the N_2O dimer. Wavefunctions of polar and nonpolar states were analyzed to assign states. In most cases, vibrational frequencies, rotational constants, and ro-vibrational transition frequencies agree well with available experimental values. For nonpolar states, differences between calculated and experimental rotational constants for all the isotopologues are similar to those previously reported for $(^{14}N_2O)_2$ in ref. 19. For polar states, the differences are also similar for isotopologues with equivalent monomers. Dimers with different monomers do not have polar states that occur in degenerate pairs with both members of each pair having wavefunction amplitude in both polar wells. Instead, the polar vibrational wavefunctions are localized in only one polar well. We find that the energy of the polar vibrational state localized above the well for which the lighter monomer has N inside is higher than the energy of the polar vibrational state localized above the well for which the heavier monomer has N inside, for both the dimers with different monomers we studied. For $^{15}N^{14}NO–^{15}N_2O$, the calculated and experimental rotational constants agree well for states localized in each of the polar wells. However, for polar states of $^{14}N_2O–^{15}N_2O$ the agreement is better for one well than for the other.

Acknowledgements

References

1 T. E. Gough, R. E. Miller and G. Scoles, *J. Chem. Phys.*, 1978, **69**, 1588–1590.

2 R. Miller, R. Watts and A. Ding, *Chem. Phys.*, 1984, **83**, 155–169.

3 R. Miller and R. Watts, *Chem. Phys. Lett.*, 1984, **105**, 409–413.

4 M. Gauthier, *J. Chem. Phys.*, 1988, **88**, 5439–5449.

5 Z. S. Huang and R. E. Miller, *J. Chem. Phys.*, 1988, **89**, 5408–5416.

6 Y. Ohshima, Y. Matsumoto, M. Takami and K. Kuchitsu, *Chem. Phys. Lett.*, 1988, **152**, 294–298.

7 B. H.-B. Qian, W. A. Herrebout and B. J. Howard, *Mol. Phys.*, 1997, **91**, 689–696.

8 A. Hecker, I. Scheele and M. Havenith, *Phys. Chem. Chem. Phys.*, 2003, **5**, 2333–2336.

9 M. Dehghani, M. Afshari, Z. Abusara, N. Moazzen-Ahmadi and A. R. W. McKellar, *J. Chem. Phys.*, 2007, **126**, 164310.

10 M. Dehghany, M. Afshari, N. Moazzen-Ahmadi and A. R. W. McKellar, *Phys. Chem. Chem. Phys.*, 2008, **10**, 1658–1661.

11 M. Dehghany, M. Afshari, Z. Abusara, C. V. Eck and N. Moazzen-Ahmadi, *J. Mol. Spectrosc.*, 2008, **247**, 123–127.

12 M. Dehghany, M. Afshari, R. Thompson, N. Moazzen-Ahmadi and A. McKellar, *J. Mol. Spectrosc.*, 2008, **252**, 1–4.

13 M. Dehghany, M. Afshari, Z. Abusara and N. Moazzen-Ahmadi, *Phys. Chem. Chem. Phys.*, 2009, **11**, 7585–7588.

14 N. R. Walker, A. J. Minei, S. E. Novick and A. C. Legon, *J. Mol. Spectrosc.*, 2008, **251**, 153–158.

15 M. Rezaei, K. H. Michaelian and N. Moazzen-Ahmadi, *J. Chem. Phys.*, 2012, **136**, 124308.

16 H. Valdes and J. A. Sordo, *J. Phys. Chem. A*, 2004, **108**, 2062–2071.

17 G. M. Berner, A. L. L. East, M. Afshari, M. Dehghany, N. Moazzen-Ahmadi and A. R. W. McKellar, *J. Chem. Phys.*, 2009, **130**, 164305.

18 R. Dawes, X.-G. Wang, A. W. Jasper and T. Carrington, Jr., *J. Chem. Phys.*, 2010, **133**, 134304.

19 X.-G. Wang, T. Carrington, Jr., R. Dawes and A. W. Jasper, *J. Mol. Spectrosc.*, 2011, **268**, 53–65.

20 L. Zheng, Y. Lu, S.-Y. Lee, H. Fu and M. Yang, *J. Chem. Phys.*, 2011, **134**, 054311.

21 M. Pavanello, L. Adamowicz, A. Alijah, N. F. Zobov, I. I. Mizus, O. L. Polyansky, J. Tennyson, T. Szidarovszky, A. G. Császár, M. Berg, A. Petrignani and A. Wolf, *Phys. Rev. Lett.*, 2012, **108**, 023002.

22 S. A. Peebles and R. L. Kuczkowski, *Mol. Phys.*, 2001, **99**, 225–237.

23 J. Tennyson and A. van der Avoird, *J. Chem. Phys.*, 1982, **77**, 5664–5681.

24 F. Gatti and C. Iung, *Phys. Rep.*, 2009, **484**, 1–69.

25 M. J. Bramley and T. Carrington, Jr., *J. Chem. Phys.*, 1993, **99**, 8519–8541.

26 G. Audi and A. Wapstra, *Nucl. Phys. A*, 1993, **565**, 1–65.

27 G. Audi and A. Wapstra, *Nucl. Phys. A*, 1995, **595**, 409–480.

28 R. A. Toth, *J. Opt. Soc. Am. B*, 1987, **4**, 357–374.

29 A. Bauer, J. Teffo, A. Valentin and T. McCubbin, *J. Mol. Spectrosc.*, 1986, **120**, 449–454.

30 X.-G. Wang and T. Carrington, Jr., *J. Chem. Phys.*, 2001, **114**, 1473–1477.

31 R. Chen and H. Guo, *J. Chem. Phys.*, 2001, **114**, 1467–1472.

32 V. A. Mandelshtam and H. S. Taylor, *J. Chem. Phys.*, 1997, **106**, 5085–5090.

33 S.-W. Huang and T. Carrington, Jr., *Chem. Phys. Lett.*, 1999, **312**, 311–318.

34 M. J. Bramley, J. W. Tromp, T. Carrington, Jr. and G. C. Corey, *J. Chem. Phys.*, 1994, **100**, 6175–6194.

35 X.-G. Wang and T. Carrington, Jr., *J. Chem. Phys.*, 2001, **115**, 9781–9796.

36 X.-G. Wang and T. Carrington, Jr., *J. Chem. Phys.*, 2003, **118**, 6946.

This journal is © the Owner Societies 2013

Phys. Chem. Chem. Phys., 2013, **15**, 19159–19168 | **19167**

37 X.-G. Wang, T. Carrington, Jr., J. Tang and A. R. W. McKellar, *J. Chem. Phys.*, 2005, **123**, 034301.

38 P. Sarkar, N. Poulin and J. T. Carrington, *J. Chem. Phys.*, 1999, **110**, 10269–10274.

39 X.-G. Wang and J. T. Carrington, *J. Chem. Phys.*, 2008, **129**, 234102.

40 H. Wei and T. Carrington, Jr., *J. Chem. Phys.*, 1992, **97**, 3029–3037.

41 J. Echave and D. C. Clary, *Chem. Phys. Lett.*, 1992, **190**, 225–230.

42 D. T. Colbert and W. H. Miller, *J. Chem. Phys.*, 1992, **96**, 1982–1991.

43 X.-G. Wang and T. Carrington, Jr., *J. Chem. Phys.*, 2004, **121**, 2937–2954.

44 R. Zare, *Angular momentum: understanding spatial aspects in chemistry and physics*, Wiley, 1988.

45 N. Walker, private communication, 2013.

46 E. Matyus, C. Fabri, T. Szidarovszky, G. Czako, W. D. Allen and A. G. Csaszar, *J. Chem. Phys.*, 2010, **133**, 034113.

19168 | *Phys. Chem. Chem. Phys.*, 2013, **15**, 19159–19168

This journal is © the Owner Societies 2013